DOI 10.1007/s10717-022-00443-y
Glass and Ceramics, Vol. 79, Nos. 1 – 2, May, 2022 (Russian Original, Nos. 1 – 2, January – February, 2022)

UDC 538.93

INFLUENCE OF GRAIN STRUCTURE FEATURES ON THE THERMOELECTRIC PROPERTIES OF COMPOUNDS BASED ON BISMUTH TELLURIDE

O. N. Ivanov,[1] M. N. Yapryntsev,[2] A. E. Vasil'ev,[1] and E. P. Dan'shina[1]

Translated from *Steklo i Keramika*, No. 1, pp. 3 – 11, January, 2022.

Original article submitted October 11, 2021

An analysis of the specific mechanisms of the influence of the state of the grain structure on the thermoelectric properties (electrical resistivity and total thermal conductivity) of the compound $Bi_{1.9}Gd_{0.1}Te_3$ is presented. The following mechanisms are considered: 1) formation of Te surface vacancies at grain boundaries, which act as donor centers; 2) change in the elemental composition of grains on high-temperature evaporation of Te on heat treatment of the material aimed at obtaining samples with a controlled average grain size.

Keywords: bismuth telluride, grain boundaries, thermoelectric properties, texturing, size effects.

Grain boundaries are an important microstructural element of ceramic functional and structural materials, whose properties are significantly affected [1 – 3]. In particular, grain boundaries can scatter electrons and phonons efficiently, which will effect the appearance of the corresponding specific mechanisms of electrical and thermal conductivity, respectively [4 – 7]. These transport properties are the most important properties of thermoelectric materials, effecting direct conversion of electric and thermic energy. Indeed, in accordance with the Ioffe formula, the thermoelectric figure of merit ZT is determined as follows:

$$ZT = S^2 \rho/(kT),$$

where ρ is the electric resistivity; S is the Seebeck coefficient; k is the total thermal conductivity, and T is the absolute temperature [8].

Low values of ρ and k must be present simultaneously in a thermoelectric material in order to increase ZT. The creation of a certain grain structure in ceramic thermoelectric materials with grains of the required shape, size, and dimensionality, as well as grain-boundary properties that determine the reflection coefficients of electrons and phonons makes it possible to partially optimize the electrical and thermal properties of materials. Grain boundaries are an important type of material defect, and the formation of a certain grain structure, which largely determines the properties of the material, corresponds to grain boundary engineering, which is one of the areas of focus in defect engineering — a powerful and effective approach to physical materials science, including thermoelectric materials science [9, 10].

At present bismuth telluride Bi_2Te_3 and compounds based on it are the main materials for low-temperature thermoelectric applications [11]. For ceramic materials, aside from the conventional mechanisms of influence of grain boundaries, on the electrical properties of Bi_2Te_3-based compounds, due to the action of grain boundaries as scattering centers, other mechanisms specific to these compounds can also appear, which, firstly, must be taken into account when analyzing the effect of the state of the grain boundary structures on the thermoelectric properties of compounds and, secondly, their use is expedient to control them by means of thermoelectric properties. These specific mechanisms are: 1) formation, at grain boundaries owing to the high-temperature evaporation of tellurium, of tellurium surface vacancies which act as donor centers affecting the concentration of free electrons in the material; 2) change in the elemental composition of the grains themselves on high-temperature evaporation of tellurium on heat treatment of the material, aimed at controlling the average grain size by choosing the required temperature and (or) duration of treatment.

[1] Shukhov Belgorod State Technological University, Belgorod, Russia (e-mail: Ivanov.Oleg@bsu.edu.ru).
[2] Belgorod State National Research University, Belgorod, Russia (e-mail: yaprintsev@bsu.edu.ru).

The purpose of the present work is a brief analysis of the listed specific mechanisms of the influence of the state of the grain structure on the electrical resistivity and total thermal conductivity of compounds based on bismuth telluride. Samples of the ceramic $Bi_{1.9}Gd_{0.1}Te_3$ were used in the investigation. In this compound, doping with gadolinium, as well as with some other rare earth elements (Lu, Tm, Ce, and others), can increase the thermoelectric figure of merit of Bi_2Te_3 [12 – 16]. However, the effect of Gd on the thermoelectric properties of bismuth telluride will not be discussed in this article.

SAMPLE PREPARATION AND PROCEDURES

The initial $Bi_{1.9}Gd_{0.1}Te_3$ powder was obtained by solvothermal synthesis. For synthesis, analytically pure grade chemical reagents were used as starting components: bismuth nitrate $Bi(NO_3)_3 \cdot 5H_2O$, tellurium dioxide TeO_2, gadolinium acetate $Gd(CH_3COO)_3 \cdot 4H_2O$, sodium hydroxide NaOH, poly(1-ethenylpyrrolidin-2-one) and ethane-1,2-diol(ethylene glycol).

The synthesis was conducted in several stages. *First step*: bismuth nitrate, tellurium oxide, and gadolinium acetate were taken in stoichiometric ratio and dissolved in a mixture of ethylene glycol (450 cm^3) and sodium hydroxide (15 g) (the mixture was constantly stirred with a magnetic stirrer). *Second step*: poly(1-ethenylpyrrolidin-2-one) was added to the resulting solution, and the reaction mixture was stirred for 30 min. *Third step:* mixture was placed in an autoclave, which was sealed and heated to temperature 190°C to initiate solvothermal synthesis. The synthesis was performed over 18 h. *Fourth step:* the synthesized dark-gray powder was separated by centrifugation and washed with deionized water and several portions of hot ethanol (to pH = 7). *Fifth step:* the powder was dried in a vacuum oven at 80°C for 8 h.

Two methods were used to obtain bulk samples. (1) Cold isostatic pressing (CIP) of the initial powder using an EPSI press at 250 MPa. The powders compacted by cold isostatic pressing were then subjected to high-temperature sintering in an argon atmosphere for 2 h. (2) Spark plasma sintering (SPS) of the initial powder using the SPS-25/10 system at 40 MPa for 5 min. The CIP method makes it possible to obtain non-textured samples with isotropic properties (CIP samples), while the SPS method yields textured samples with anisotropic properties (SPS samples). In addition, to obtain textured and non-textured samples with different grain structures differing in average grain size, the sintering temperature T_S was varied in both methods. The temperature T_S for CIP samples was changed as follows: T_S = 690, 720, 735, 750, 780, and 810 K; for SPS samples: T_S = 690, 720, 750, 780, and 810 K.

Scanning electron microscopy (Quanta 600 microscope) and optical emission spectrometry with inductively coupled plasma (ICPE-9000 spectrometer) were used as the main methods of investigating the microstructure and elemental composition of the samples. To determine the Lotgering factor, which characterizes the degree of texturing, diffractograms were taken using a Rigaku SmartLab x-ray diffractometer (CuK_α radiation). The ZEM-3 measurement system was used to measure the electrical resistance by the four-probe method, and the TC-1200H system was used to measure the total thermal conductivity by the laser flash method. To determine the concentration of major carriers, the Hall effect was studied using a Cryogen Free system.

EXPERIMENTAL RESULTS

Characterization of the grain structure of CIP and SPS $Bi_{1.9}Gd_{0.1}Te_3$ samples. The certification results for the initial $Bi_{1.9}Gd_{0.1}Te_3$ powder used for the preparation of CIP and SPS samples are given in [17]. The powder was single-phase with a crystal structure corresponding to the Bi_2Te_3 structure and consisted of particles having the shape of hexagonal plates with transverse dimensions of several hundreds of nanometers and thickness about 100 nm (i.e., the particles of the initial powder are two-dimensional).

In the process of cold isostatic pressing, the same pressure is applied to the body compacted from the initial powder from all directions [17, 18]. With such pressing, the compacted body will be compressed uniformly. As a result, after sintering, an isostatically compacted material will have grain structure with random grain orientation, although the grains themselves may remain highly anisotropic in shape. The images obtained by scanning electron microscopy (SEM images) of the surface cleavage of $Bi_{1.9}Gd_{0.1}Te_3$ CIP samples sintered at 690 and 810 K are shown in Fig. 1*a* and *b*, respectively. It can be seen, firstly, that the grains are in the form of plates; secondly, the plates themselves are randomly arranged; and, thirdly, the grain size noticeably increases with increasing sintering temperature.

In the spark plasma sintering process based on uniaxial pressing, a texture associated with partial grain ordering develops in the material sintered from the initial powder [18, 19]. In the texturing process, the grains will be located mainly in a plane perpendicular to the direction of application of uniaxial pressure during sintering. In this case, the direction of pressure application will be the axis of the texture.

Texturing is easily observed in SEM images of the grain structure obtained from surface cleavages perpendicular or parallel to the texture axis. Such images for SPS $Bi_{1.9}Gd_{0.1}Te_3$ samples are shown in Fig. 1*c* and *d*. The grain structure in the image of a parallel surface is the so-called lamellar structure.

The lamellar layers themselves consist of elongated grains. The grain structure in the image of a perpendicular surface is characterized by grains of irregular shape, which are randomly arranged. It is important that the grain sizes in $Bi_{1.9}Gd_{0.1}Te_3$ SPS samples in directions parallel and perpendicular to the texture axis will differ from each other. To determine the average grain size in CIP and SPS samples depending on the sintering temperature, we analyzed the plot-

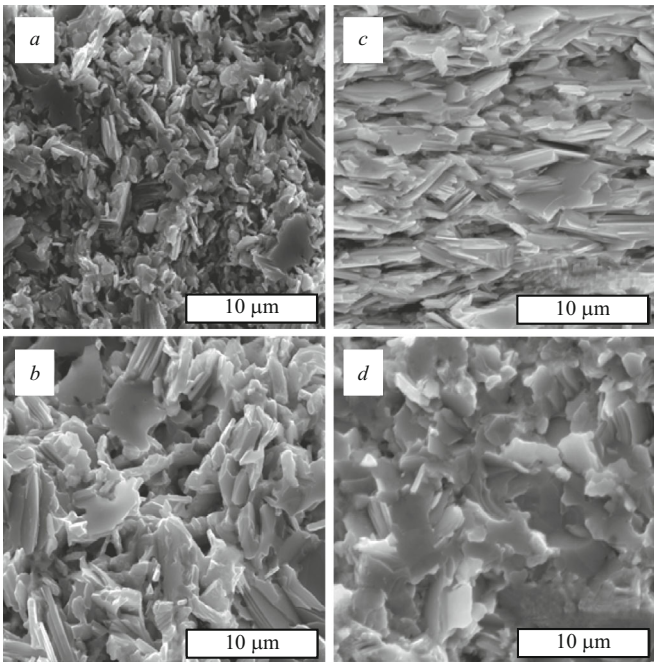

Fig. 1. SEM images of a surface cleavage of CIP samples sintered at (*a*) 690 and (*b*) 810 K and a surface cleavage of SPS samples oriented perpendicular (*c*) and parallel (*d*) to the direction of pressure application during spark plasma sintering.

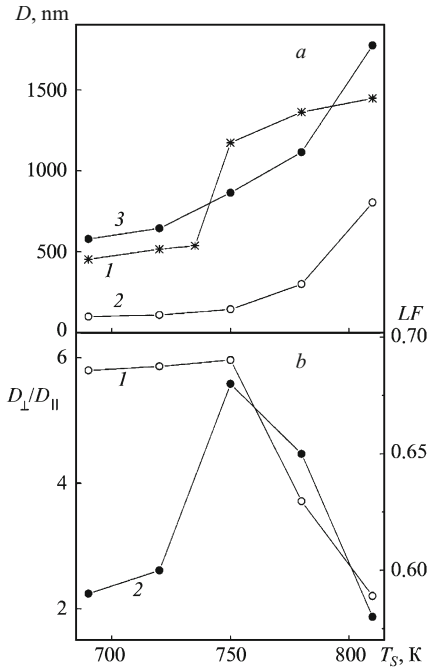

Fig. 2. Effect of sintering temperature on the average grain size D of CIP samples (curve *1*) and SPS samples; curves *2* and *3* correspond to the average grain sizes determined in directions perpendicular $D_\perp$ and parallel $D_\parallel$ to the direction of pressure application during spark plasma sintering (*a*); influence of sintering temperature on grain shape factor $D_\parallel / D_\perp$ (*1*) and Lotgering factor (*b*).

ted grain size distribution histograms. As a result, estimates of the average isotropic grain size D for CIP samples were obtained, as well as the average grain sizes for SPS samples in directions parallel ($D_\parallel$) and perpendicular ($D_\perp$) to the texture axis.

The dependences of D, $D_\parallel$, and $D_\perp$ on the sintering temperature are shown in Fig. 2*a*. Clearly, all three average sizes increase with increasing sintering temperature. Grain growth at high temperatures in bulk materials sintered from a pre-compacted initial powder is a well-known physical phenomenon. It is associated with energy reduction of the sintered powder as a substantially inhomogeneous system with numerous interparticle (grain) boundaries, which are interfaces in the system [20]. The energy of such interfaces can be expressed as γA (γ is the specific energy of the surface and A is the surface area). The particles of the initial powder will retain their shape in the process of obtaining the final polycrystalline (ceramic) material.

However, the surface area reduction of the particles during sintering occurs as a result of the coalescence of the particles, effecting an increase in their size. For ICP samples, the dependences $D_\parallel(T_S)$ and $D_\perp(T_S)$ are smooth curves, while for CIP samples, the dependence $D(T_S)$ shows a stepwise reduction in D above $T_S = 735$ K. This behavior of $D(T_S)$ makes it possible to conditionally divide all CIP samples into two groups: fine- and coarse-grained samples. Fine-grained samples should include samples sintered at 690, 720, and 735 K (for these samples, the average grain size is about 500 nm and weakly depends on the sintering temperature). In coarse-grained samples sintered at 750, 780, and 810 K, the average grain size is greater than 1100 nm and increases significantly on sintering above 750 K. For ICP samples, $D_\perp$ is larger than $D_\parallel$. These sizes can be used to quantify the shape of a grain using the shape factor, defined as the ratio $D_\perp / D_\parallel$. Obviously, the greater the value of $D_\perp / D_\parallel$, the more the grain will correspond in shape to a two-dimensional object.

The dependence of the grain shape factor on the sintering temperature is shown by curve *1* in Fig. 2*b*. It is evident that for $T_S \le 690$, 720, and 750 K the grain shape factor $D_\perp / D_\parallel$ is quite high. This means that grains with such a shape factor can be considered as two-dimensional objects. However, for sintering temperatures above 750 K the values of $D_\perp / D_\parallel$ gradually fall, which is associated with a change in the shape of the grain from a two-dimensional to a three-dimensional object. Such a change in the grain shape could be due to the fact that the rate of grain growth during sintering in different directions (parallel and perpendicular to the texture axis) also turns out to be different. Indeed, the rate of high-temperature grain growth in SPS samples in the direction parallel to the direction of pressure application turns out to be higher than for the perpendicular direction.

The degree of grain ordering in textured SPS samples was estimated using the Lotgering factor LF [18]. The factor LF was calculated from the diffraction patterns for SPS sam-

ples sintered at different temperatures. The development of texturing in compounds based on Bi_2Te_3 manifests itself in different forms of diffraction patterns taken from surfaces oriented perpendicularly or parallel to the direction of pressure application (texture axis). Although the positions of the x-ray reflection intensity peaks on the diffraction patterns do not depend on the direction of pressure application, the intensity values of certain peaks will depend on this direction as follows: the intensities of the peak (00l) will increase on the 'perpendicular' diffraction pattern and become narrower on the 'parallel' diffraction pattern. The intensities of the peak (11l) will increase. Such a redistribution of intensities is fully consistent with the formation of a texture with an ordered grain structure. The Lotgering factor was calculated by the formula

$$LF = \frac{p - p_0}{1 - p_0}, \quad (1)$$

where p and p_0 are defined as

$$p = \frac{I(00l)}{\sum I(hkl)}; \quad p = \frac{I_0(00l)}{\sum I_0(hkl)}, \quad (2)$$

where h, k, and l are the Miller indices of the respective reflection planes.

Here the intensities I and I_0 correspond to textured and untextured samples, respectively. Ideally, $F = 1$ for a fully oriented sample and $F = 0$ for a completely unoriented sample.

Curve *2* in Fig. 2 shows the dependence of LF on the sintering temperature for SPS samples. With an increase in the sintering temperature, The Lotgering factor increases with increasing sintering temperature for $T_S \le 750$ K but decreases above 750 K. This signifies that the material's ability to be textured is related with the grain shape factor $D_\perp / D_\parallel$. The more pronounced the anisotropy of the grain shape (i.e. the greater the ratio $D_\perp / D_\parallel$) in the samples, the greater their texturing.

Formation of Te surface vacancies at grain boundaries of CIP and SPS $Bi_{1.9}Gd_{0.1}Te_3$ samples acting as donor centers. It is known that the type (electrons or holes) and concentration of current carriers in compounds based on Bi_2Te_3 are determined by different types of point defects [21 – 23]. Characteristic defects for these compounds are $V_{Te}^{\bullet\bullet}$ tellurium vacancies formed in high-temperature processes in obtaining such compounds. This is due to the fact that the evaporation energy of tellurium ($52.55\ kJ \cdot mol^{-1}$) is much less than the evaporation energy of bismuth ($104.80\ kJ \cdot mol^{-1}$). As a result, on high-temperature sintering Te evaporates faster than Bi does, which is accompanied by the formation of $V_{Te}^{\bullet\bullet}$ vacancies. To compensate the positive electric charge of a vacancy $V_{Te}^{\bullet\bullet}$ in the bulk of the material (restoration of electric neutrality), two free electrons (conduction electrons) will be formed on formation of each vacancy in accordance with the expression

$$Bi_2Te_3 = 2Bi_{Bi}^{\times} + 2Te_{Te}^{\times} + Te(g) + V_{Te}^{\bullet\bullet} + 2e', \quad (3)$$

where the symbol g corresponds to the gas phase. In polycrystalline (ceramic) compounds based on Bi_2Te_3, Te will evaporate predominantly from grain boundaries, leading primarily to the formation of surface vacancies $V_{Te}^{\bullet\bullet}$. These vacancies can be considered as partial, in contrast to full (bulk) vacancies $V_{Te}^{\bullet\bullet}$. Partial vacancies also act as donor centers, and the number of free electrons generated by such centers is determined by the number of dangling chemical bonds formed on formation of a vacancy. The formation of partial vacancies $V_{Te}^{\bullet\bullet}$ leads to the fact that electrons are the main current carriers in Bi_2Te_3-based polycrystalline compounds [22]. Since partial surface vacancies $V_{Te}^{\bullet\bullet}$ influence the electron concentration n, the n in CIP and SPS samples of $Bi_{1.9}Gd_{0.1}Te_3$ can be expected to depend on the grain boundary density (number of grain boundaries per unit volume). The reciprocal of the average grain size can be used as a rough estimate of such density. The larger $1/D$, i.e. the smaller D, the greater the density of grain boundaries, and vice versa. Dependences $n(1/D)$ for CIP samples and $n(1/D_\perp)$ for SPS samples displayed in Fig. 3.

It is evident in Fig. 3 that for all samples the electron concentration actually decreases with increasing density of grain boundaries, which may be due to the presence of surface partial vacancies $V_{Te}^{\bullet\bullet}$. The dependences $n(1/D)$ and $n(1/D_\perp)$ are close to linear.

For CIP samples, it was found that the concentration of conduction electrons decreases on switching from fine- to coarse-grained samples. Thus, grain boundaries can significantly affect the electrical properties of Bi_2Te_3-based compounds not only through a change in the mobility of electrons, acting as effective electron scattering centers, but also through a change in the electron concentration, acting as a collection of donor centers (surface partial vacancies $V_{Te}^{\bullet\bullet}$).

Change in the elemental composition of grains on high-temperature evaporation of Te during heat treatment of CIP and SPS samples of $Bi_{1.9}Gd_{0.1}Te_3$. An obvious technological method of obtaining ceramic samples of various materials with a controlled average grain size is high-temperature treatment, which effects recrystallization and grain growth [24]. The grain size can be controlled by appropriate selection of temperature and/or duration of treatment. Figure 2*a* shows that high-temperature grain growth actually occurs on sintering of CIP and SPS samples of $Bi_{1.9}Gd_{0.1}Te_3$. An increase in the sintering temperature effects the expected increase in the average grain size, so that $Bi_{1.9}Gd_{0.1}Te_3$ samples with the desired grain size can be obtained by choosing the correct parameters for their preparation. However, because of the high-temperature evaporation of Te, an important feature of compounds based on Bi_2Te_3 is

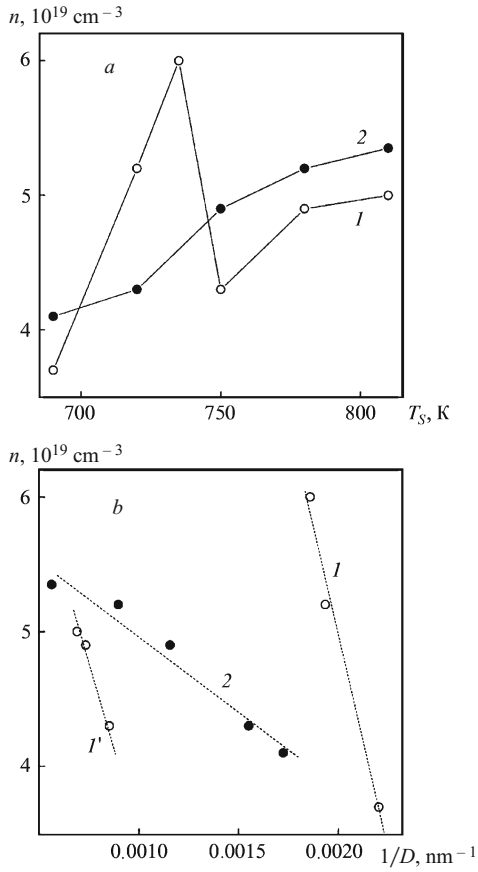

Fig. 3. Influence of sintering temperature on the electron concentration in CIP samples — curve *1* and SPS samples — curve *2* (*a*) and the dependence of the electron concentration on the reciprocal value of the average grain size in CIP samples with fine-grained (curve *1*) and coarse-grained (curve *1'*) structures and in SPS samples (curve *2*) (*b*).

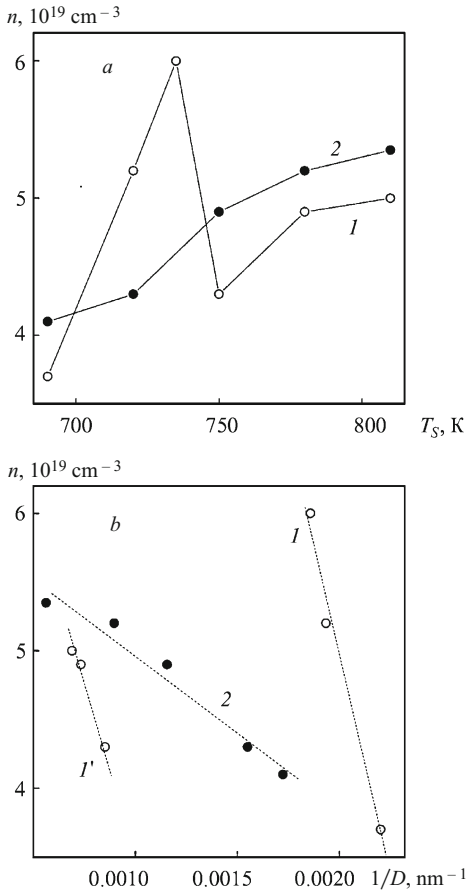

Fig. 4. Effect of sintering temperature on the Te content in CIP samples (curve *1*) and SPS samples (curve *2*) (*a*), dependence of the electron concentration on the Te content in CIP samples (curve *1*) and SPS samples (curve *2*) (*b*), Te content in CIP samples and SPS samples (curves *2* and *3* correspond to the average grain sizes determined in directions perpendicular and parallel to the direction of pressure application during spark plasma sintering) with different average grain sizes (*b*).

associated with a change in their elemental composition during the preparation process. As noted above, the evaporation of Te leads to the formation of bulk and surface vacancies $V_{Te}^{\bullet\bullet}$ that act as donor centers.

In this case, in analyzing the change in the concentration of conduction electrons, it is necessary to take into account not only the contribution of grain boundaries containing surface vacancies $V_{Te}^{\bullet\bullet}$ but also the total contribution of bulk and surface vacancies $V_{Te}^{\bullet\bullet}$. In other words, in the process of obtaining compounds based on Bi_2Te_3 with controlled grain size (due to high-temperature treatment), it is necessary to take into account the amount of Te remaining in the samples after treatment, which will be determined for a given grain structure formed as a result of treatment.

The effect of the sintering temperature on the Te content in CIP and SPS samples of $Bi_{1.9}Gd_{0.1}Te_3$ samples is shown in Fig. 4*a*. A Te deficiency is observed in all samples; the samples are nonstoichiometric in tellurium (the stoichiometric composition is characterized by Te content equal to 60 at.%). Moreover, the deviation from stoichiometry increases with increasing sintering temperature. Figure 4*b* illustrates how the electron concentration depends on the Te content. For CIP samples, *n* increases with decreasing Te content in two regions corresponding to fine- and coarse-grained samples, but on switching from fine- to coarse-grained samples the electron concentration noticeably decreases (as discussed above, this is due to density reduction of grain boundaries containing donor centers — surface partial vacancies $V_{Te}^{\bullet\bullet}$). For SPS samples, *n* increases non-monotonically with decreasing Te content. The complex behavior of *n* versus the Te content is associated with the simultaneous action of bulk and partial vacancies $V_{Te}^{\bullet\bullet}$ as donor centers. Moreover, aside from the formation of these vacancies, antisite defects Bi_{Te} (when a Bi atom occupies the Te position in the crystal structure) can form in Bi_2Te_3-based compounds [25]. On formation of each antisite defect one hole appears as a minority current carrier, which compensates for the negative charge of free electrons as the main current carriers.

As noted earlier, during high-temperature processing of compounds based on Bi_2Te_3, each sample with a certain grain size will correspond to a certain Te content. Thus, at high temperatures grain growth and tellurium evaporation occur simultaneously. Figure 4*c* confirms this conclusion for the CIP and SPS $Bi_{1.9}Gd_{0.1}Te_3$ samples. Indeed, it is clear from the figure that, depending on the sintering temperature, a grain structure with a certain value of the average grain size and tellurium content is formed in the samples.

CONCLUSIONS

The specific mechanisms of the effect of grain structure features on electrical resistivity and total thermal conductivity of samples of Bi_2Te_3-based thermoelectric materials were investigated in untextured and textured samples of $Bi_{1.9}Gd_{0.1}Te_3$ with *n*-type conductivity. The specific mechanisms are: 1) the formation of surface tellurium vacancies at grain boundaries, which act as donor centers and increase the concentration of free electrons; 2) change in the elemental composition of grains during the evaporation of Te on high-temperature processing of the material, which makes it possible to obtain samples with a controlled average grain size. These mechanisms must be taken into account in order to obtain Bi_2Te_3-based compounds with a high thermoelectric figure of merit.

The work was supported by the Ministry of Education and Science of the Russian Federation, project No. 0625-2020-0015.

REFERENCES

1. T. Watanabe, "Grain boundary engineering: Historical perspective and future prospects," *J. Mater. Sci.*, **46**, 4095 – 4115 (2011).
2. I. P. Semenova, R. Z. Valiev, E. B. Yakushina, et al., "Strength and fatigue properties enhancement in ultrafine-grained Ti produced by severe plastic deformation," *J. Mater. Sci*., **4**, 7354 – 7359 (2008).
3. N. Vandewalle, G. Lumay, O. Gerasimov, and F. Ludewig, "Influence of grain shape, friction and cohesion on granular compaction dynamics," *Eur. Phys. J. E.*, **22**, 241 – 248 (2007).
4. O. Ivanov, O. Maradudina, and R. Lyubushkin, "Grain size effect on electrical resistivity of bulk nanograined Bi_2Te_3 material," *Mater. Charact*., **99**, 175 – 179 (2015).
5. W. Kim, "Strategies for engineering phonon transport in thermoelectrics," *J. Mater. Chem. C*, No. 3, 10336 – 10348 (2015). URL: https://doi: 10.1039/C5TC01670C
6. D. Choi, "The electron scattering at grain boundaries in tungsten films," *Microelectron. Eng.*, **122**, 5 – 8 (2014).
7. H. Wu, J. Carrete, Z. Zhang, et al., "Strong enhancement of phonon scattering through nanoscale grains in lead sulfide thermoelectrics," *NPG Asia. Mater.*, **6**, 2 – 11 (2014).
8. G. J. Snyder, "Figure of merit ZT of a thermoelectric device defined from materials properties," *Energy Environ. Sci*., **10**, 2280 – 2283 (2017).
9. Y. Zheng, T. J. Slade, L. Hu, et al., "Defect engineering in thermoelectric materials: what have we learned?," *Chem. Soc. Rev.*, **50**, 9022 – 9054 (2021).
10. C. Zhou, Y. K. Lee, J. Cha, et al., "Defect engineering for high-performance *n*-type PbSe thermoelectrics," *J. Am. Chem. Soc*., **140**, 9282 – 9290 (2018).
11. H. J. Goldsmid, "Bismuth telluride and its alloys as materials for thermoelectric generation," *Mater.*, **7**, 2577 – 2592.
12. F. Wu, W. Shi, and X. Hu, "Preparation and thermoelectric properties of flower-like nanoparticles of Ce-doped Bi_2Te_3," *Electron. Mater. Lett*., **11**, 127 – 132 (2015).
13. J. Yang, F. Wu, Z. Zhu, et al., "Thermoelectrical properties of lutetium-doped Bi_2Te_3 bulk samples prepared from flower-like nanopowders," *J. Alloys Compd.*, **619**, 401 – 405 (2015).
14. X. H. Ji, X. B. Zhao, Y. H. Zhang, et al., "Synthesis and properties of rare earth containing Bi_2Te_3 based thermoelectric alloys," *J. Alloys Compd*., **387**, 282 – 286 (2005).
15. F. Wu, H. Song, J. Jia, and X. Hu, "Effects of Ce, Y, and Sm doping on the thermoelectric properties of Bi_2Te_3 alloy," *Prog. Nat. Sci. Mater. Int*., **23**, 408 – 412 (2013).
16. F. Wu, H. Z. Song, J. F. Jia, et al., "Thermoelectric properties of Ce-doped *n*-type $Ce_xBi_{2-x}Te_{2.7}Se_{0.3}$ nanocomposites," *Phys. Stat. Sol. A*, **210**, 1183 – 1189 (2013).
17. M. Yapryntsev, A. Vasil'ev, and O. Ivanov, "Sintering temperature effect on thermoelectric properties and microstructure of the grained $Bi_{1.9}Gd_{0.1}Te_3$ compound," *J. Europ. Cer. Soc.*, **39**, 1193 – 1205 (2019).
18. O. Ivanov, M. Yaprintsev, and A. Vasil'ev, "Comparative analysis of the thermoelectric properties of the non-textured and textured $Bi_{1.9}Gd_{0.1}Te_3$ compounds," *J. Sol. St. Chem*., **290**, 121559 – 121658 (2020).
19. M. Yaprintsev, A. Vasil'ev, and O. Ivanov, "Thermoelectric properties of the textured $Bi_{1.9}Gd_{0.1}Te_3$ compounds spark-plasma-sintered at various temperatures," *J. Europ. Cer. Soc*., **40**, 742 – 750 (2020).
20. J. K. L. Lai, C. H. Shek, and G. M. Lin, "Grain growth kinetics of nanocrystalline SnO_2 for long-term isothermal annealing," *Sci. Mater.*, **49**, 441 – 446 (2003).
21. Y. Pan, T. R. Wei, C. F. Wu, and J. F. Li, "Electrical and thermal transport properties of spark plasma sintered *n*-type $Bi_2Te_{3-x}Se_x$ alloys: the combined effect of point defect and Se content," *J. Mater. Chem. C*, **3**, 10583 – 10589 (2015).
22. L. Hu, T. Zhu, X. Liu, and X. Zhao, "Point defect engineering of high-performance bismuth-telluride-based thermoelectric materials," *Adv. Funct. Mater.*, **24**, 5211 – 5218 (2014).
23. J. Suh, K. M. Yu, D. Fu, et al., "Simultaneous enhancement of electrical conductivity and thermopower of Bi_2Te_3 by multifunctionality of native defects," *Adv. Mater.*, **27**, 3681 – 3686 (2015).
24. F. J. Humphreys and M. Hatherly, *Recrystallization and Related Annealing Phenomena*, Elsevier, Oxford (2004).
25. J. Lee, A. Berger, L. U. Cagnon, et al., "Disproportionation of thermoelectric bismuth telluride nanowires as a result of the annealing process," *Phys. Chem. Chem. Phys.*, **12**, 15247 – 15250 (2010).